Chapter 9
Implementation of QTLC Systems

9.1 Introduction

Optical communications appear as a natural evolution of digital radio frequency (RF) communications. This evolution implied a change of the frequency range of the carrier from about 10^9 Hz for radio and microwave communications to about 10^{15} Hz for optical communications (see also Sect. 4.4). The major advantage in using optical frequencies is related to the possibility of utilizing the enormous bandwidths available in the optical spectrum. Of course, owing to the very small wavelengths involved, a completely different technology was needed for the development of optical communications.

A fundamental role in optical technology has been played by the invention of laser around 1960. This component is a high-powered, almost monochromatic and very directive source, whose advent suggested the possibility of its use in long-distance optical transmissions. Indeed, the high directivity of this new source allows huge antenna gains. On the other hand, the hope related to the advent of the laser appeared somewhat cooled down by the presence of the atmospheric turbulence, a phenomenon caused by interaction of the light with the atoms. The development of optical fibers enabled the experimenters to use a waveguided channel, practically insensitive to interferences with the surrounding environment. This fact gave new impetus to optical communications, with a wide range of practical applications in the field of terrestrial communications.

Another fundamental difference between radio and optical communications arises from the fact that at optical frequencies it is not possible the use of antennas extracting an electrical signal from the electromagnetic field and only detectors sensitive to the field intensity, as photodetectors, are available. Fortunately, the development of photodetection devices as the avalanche photodetectors (APD) combined with the high energy of laser beam made possible the combination of the simplest modulation (intensity modulation) with the direct detection of the signal energy. This approach, not possible at radio frequency, has been largely utilized in terrestrial fiber optics. Moreover, usual means of the radio frequency communications as phase modulation

G. Cariolaro, *Quantum Communications*, Signals and Communication Technology,
DOI 10.1007/978-3-319-15600-2_9

and coherent detection can be employed in optical communications to improve the performances of the direct detection.

9.1.1 The System Model

The first optical communication systems mimicked the well-known radio frequency techniques. This gave rise to classical optical systems as incoherent detection and homodyne detection. These systems are perfectly adequate to the needs of the optical communications as long as the received field is so large that the quantum effects are negligible. On the other hand, in applications as deep space communications, the received field may be so weak that quantum effects dominate and a clear advantage is obtained using quantum detection approaches. Moreover, in other applications as quantum key distribution, the use of weak fields with quantum detection becomes essential to guarantee the security of the transmission.

As we have seen in the previous chapters, the block diagram of a point-to-point optical communications system is by no means different from the standard model and is given by the cascade of a transmitter, a physical channel, and a receiver.

The **optical transmitter** is composed of the cascade of an optical source, a modulator, and a coupling device adapting the beam to the optical transmission medium. The source (a laser) generates an electromagnetic field in the optical range. The modulator, on the basis of the digital information to be transmitted, modifies a parameter (usually the amplitude or the phase) of the electromagnetic field.

The **physical transmission channel** may be the free space or an optical fiber. On the choice of the medium is based a rough classification into **guided** and **unguided** optical transmission systems.

Finally, the **optical receiver** is the cascade of a coupling device, a demodulator, and a photodetector. The demodulating device, if any, combines the received optical field with a locally generated field. The photodetector converts the optical signal into an electric signal for the postdetection processing.

The main difference between free space and guided transmission systems resides in the coupling approach of the laser beam to the optical medium. In free space systems (Fig. 9.1) at the transmitter side an optical antenna focuses the field into a narrow beam. At the receiver side, another optical antenna refocuses the electromagnetic beam, possibly spread by the medium, into the detection surface (see also Sect. 4.4.5). In optical fiber transmissions (Fig. 9.2) the couplings laser–fiber and fiber–detector are realized via fiber connections, adapters, or optical lenses.

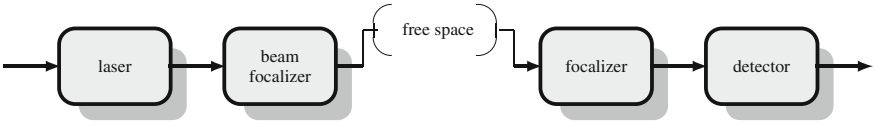

Fig. 9.1 Scheme of quantum optical system in the free space

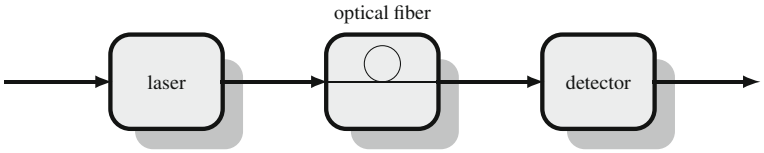

Fig. 9.2 Scheme of quantum optical guided system

9.1.2 Outline of the Chapter

In Sect. 9.2 we present the basic components of optical communication systems, namely, laser, modulators, beam splitters, and photodetectors. In particular, we give their models both from the classical and the quantum point of view. In Sect. 9.3, the major classical optical communication schemes (direct detection and homodyne detection) are presented with their quantum equivalent models.The limits of classical optical communications (shot noise limit and standard quantum limit) are introduced. In Sect. 9.4 the most popular binary quantum communication schemes are presented, starting from the Kennedy and the Sasaki–Hirota receivers. Particular attention is devoted to the analysis and interpretation of the Dolinar receiver, that attains the Helstrom bound. In Sect. 9.5 recent evolutions toward suboptimal K-ary systems are presented. In particular, multidisplacement receivers for K-PSK and K-QAM are outlined. Finally, some results on possible implementations of PPM receivers are presented.

Advice to the reader. Some topics of this chapter imply the knowledge of the continuous variables, whose fundamentals are developed in Chap. 11. Then, we strongly recommend the reader to revisit the present chapter after an adequate comprehension of some topics of Chap. 11, as bosonic operators and displacement and rotation transformations.

9.2 Components for Quantum Communications Systems

As noted in the introduction, the main components of the optical communication systems are the laser and the photodetector. Other components, as modulators, lenses, and mirrors, are used in order to improve the communication performances through modulation and demodulation techniques.

In this section, a summary description of the main components of the transmitter and the receiver of quantum communications systems is given.

9.2.1 Laser

The key component of all quantum communications systems is the laser, that provides the physical carrier for the information transmission. For a detailed analysis of principles and applications the reader may see for instance [1].

From a physical point of view, the laser is a narrow band optical amplifier with amplification provided by an active medium excited by an external source of energy (the **pump** in the technical jargon). As in many electrical oscillators, optical oscillation arises as a combined effect of the spontaneous photon emission of the active medium and of the feedback provided by an optical cavity. In order that the oscillation may start, the pump power must be above a threshold assuring that the gain of the active medium is greater than the loss. Moreover, the length of the cavity must be matched to the natural laser wavelength.

From a classical point of view, the radiation produced by a laser can be modeled as an electromagnetic wave with electric field

$$\mathbf{E}(r,t) = E_0[\,\alpha(r,t)\mathrm{e}^{\mathrm{i}2\pi\nu t} + \alpha^*(r,t)\mathrm{e}^{-\mathrm{i}2\pi\nu t}\,]\mathbf{p}(r,t) \tag{9.1}$$

originating as a single mode solution of the wave equation into the cavity and propagating in the external space along some direction z, with optical frequency ν. The vector $\mathbf{p}(r,t)$ takes into account the field polarization. The complex amplitude $\alpha(r,t)$ can be written as

$$\alpha(r,t) = \alpha_0(r)\mathrm{e}^{\mathrm{i}\phi(r,t)}, \tag{9.2}$$

where $\phi(r,t)$ is the time and space-dependent phase. In the simplest case, known as Gaussian beam, the amplitude $\alpha_0(r)$ has circular symmetry in the plane orthogonal to the propagation axis z and is given by

$$\alpha_0(r) = \frac{\alpha_0}{z + \mathrm{i}z_0}\exp\left(-\frac{\mathrm{i}(x^2+y^2)}{2(z+\mathrm{i}z_0)}\right), \qquad r = (x,y,z), \tag{9.3}$$

where α_0 and z_0 are real constants. The corresponding intensity is

$$I(r) = \frac{\alpha_0^2}{z^2+z_0^2}\exp\left(-\frac{z_0^2(x^2+y^2)}{z^2+z_0^2}\right). \tag{9.4}$$

This beam has the nice property that its shape remains unchanged in reflection and diffraction.

The field (9.1) may be put in the form

$$E(r,t) = [\,x_1(r,t)\cos(2\pi\nu t) + x_2(r,t)\sin(2\pi\nu t)]\,\mathbf{p}(r,t), \tag{9.5}$$

where the quadrature components x_1 and x_2 are in evidence. It can be proved that x_1 and x_2 have the same properties of the position q and the momentum p of a mechanical harmonic oscillator (see Sect. 11.3). Then, from a quantum point of view, after a suitable normalization, the components x_1 and x_2 are substituted by two quantum observables q and p satisfying the canonical correlation condition $[\,q\,,\,p\,] = 2\mathrm{i}$. Equivalently, $\alpha(r,t)$ and its conjugate are substituted by the bosonic operators a and a^* satisfying the correlation condition $[\,a, a^*\,] = 1$ and operating in the Fock space. The formalization of these ideas will be seen in the context of continuous variables (Chap. 11), where the radiation emitted by a laser is modeled as a coherent state.

9.2.2 Beam Splitter

The beam splitter is a partially transmitting mirror (Fig. 9.3) which combines two optical beams impinging orthogonally on the mirror surface. In the case of fiber links, the device with the same role is called *fiber combiner* or *fiber coupler*, and it is usually obtained by fusing together the core of two fiber patches.

The classical model of the beam splitter, known from the nineteenth century, is as follows. We assume that the input beams have the same frequency and amplitudes α and β. Then the output beams α' and β' are related to α and β by the relations

$$\begin{aligned} \alpha' &= \sqrt{1-\tau}\,\alpha + \sqrt{\tau}\,\beta \\ \beta' &= \sqrt{\tau}\,\alpha - \sqrt{1-\tau}\,\beta \end{aligned} \tag{9.6}$$

where phases have been neglected for simplicity. Since

$$|\alpha'|^2 + |\beta'|^2 = |\alpha|^2 + \beta|^2, \tag{9.7}$$

the device is lossless. The meaning of the parameter τ is apparent. If $\beta = 0$, one gets $|\alpha'|^2 = (1-\tau)|\alpha|^2$ and $|\beta'|^2 = \tau|\alpha|^2$. Then τ is the fraction of the power transmitted

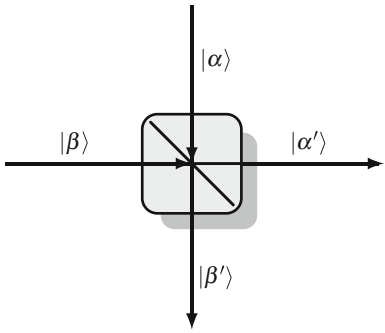

Fig. 9.3 Beam splitter with the input kets $|\alpha\rangle$ and $|\beta\rangle$ and the output kets $|\alpha'\rangle$ and $|\beta'\rangle$

through the mirror and is called the **transmissivity** of the beam splitter. If the device introduces losses due to absorption and scattering, the previous equation becomes

$$|\alpha'|^2 + |\beta'|^2 = (1 - L)(|\alpha|^2 + \beta|^2). \tag{9.8}$$

On the other hand values of L below 10^{-4} have been achieved, so that in a first approximation losses may be neglected.

For a detailed analysis of the quantum model of the beam splitter in the context of continuous variables the reader is referred to Sect. 11.17.5. Here we confine us to observe that the Heisenberg representation of the input–output relations of the beam splitter is obtained by the classical model by substituting the field amplitudes with the annihilation operators corresponding to the beams, namely,

$$\begin{aligned} a' &= \sqrt{1-\tau}a + \sqrt{\tau}b \\ b' &= \sqrt{\tau}a - \sqrt{1-\tau}b \end{aligned} \tag{9.9}$$

where a and b are the annihilation operators of the input beams and a' and b' are the annihilation operators of the output beams.

Note that in the quantum model the presence of both beams is mandatory to correctly describe such a two-input two-output device. Indeed, if we ignore the annihilator b, we would have for instance $[\,a', a'^*\,] = (1 - \tau)[\,a, a^*] = (1 - \tau)$ in contradiction with the bosonic commutation rule. Taking into account b one gets

$$[\,a', a'^*\,] = (1 - \tau)[\,a, a^*\,] + \tau[\,b, b^*\,] = 1 \tag{9.10}$$

and the commutation relation is satisfied.

In the Schrödinger representation corresponding to the Heisenberg representation (9.9) (see Sect. 3.4) in the case of coherent states, the beam splitter transforms the input joint state $|\alpha\rangle \otimes |\beta\rangle$ to the output joint state $|\alpha'\rangle \otimes |\beta'\rangle$ with

$$\begin{aligned} |\alpha'\rangle &= |\sqrt{1-\tau}\alpha + \sqrt{\tau}\beta\rangle \\ |\beta'\rangle &= |\sqrt{\tau}\alpha - \sqrt{1-\tau}\beta\rangle \end{aligned} \tag{9.11}$$

in perfect analogy with the classical interpretation.

One of the most important application of the beam splitter in optical technique is the **approximate realization of the quantum displacement**. If we apply to the second input the coherent state $|\gamma\rangle = |\beta/\sqrt{\tau}\rangle$, the coherent state at the first output becomes

$$|\sqrt{1-\tau}\alpha + \gamma\rangle \tag{9.12}$$

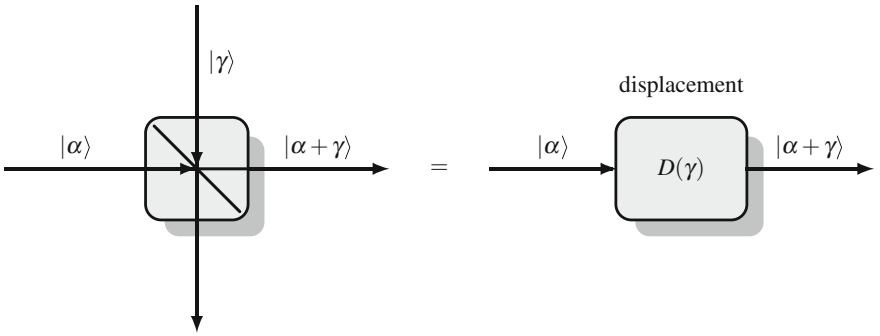

Fig. 9.4 Approximate realization of a *displacement* through a *beam splitter* (the second output of the beam splitter is not used)

approximating $|\alpha+\gamma\rangle = D(\gamma)|\alpha\rangle$ as $\tau \to 0$ (Fig. 9.4). Then, a displacement of amplitude γ may be obtained, at least approximately, with a beam splitter of low transmissivity τ driven at the second input by a high level coherent state $|\beta/\sqrt{\tau}\rangle$.

The theory of the beam splitter, formulated as a two-mode unitary operator, will be seen in Sect. 11.17.

9.2.3 Modulators

Essentially, we have *phase* modulators and *amplitude* modulators, which provide the relations

$$|\psi\rangle \quad \to \quad |\mathrm{e}^{\mathrm{i}\,\phi}\,\psi\rangle\,, \qquad |\psi\rangle \quad \to \quad |A\,\psi\rangle\,. \tag{9.13}$$

The corresponding graphical representation is illustrated in Fig. 9.5. The amplitude modulators are obtained with attenuation ($A < 1$).

In quantum transmission systems, intensity and phase modulation may be obtained by exploiting electro-optical properties of particular crystals, in which the refractive index depends on the intensity of the electric field applied to the material. Then, the

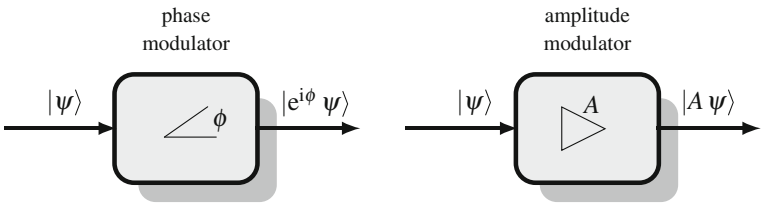

Fig. 9.5 Graphical representation of phase and amplitude modulators

phase of the output beam may be modulated by varying an electric voltage applied to the device.

Different mechanisms are used to modify the refractive index of the crystal. Electro-optic modulators exploit the so-called *Pockels cells*, waveguide made of nonlinear crystal material which can be considered equivalent to voltage-controlled waveplates. The variable electric voltage drives the phase delay induced to the optical beam traveling through the modulator.

Depending on the direction of the applied electric field, the type and the orientation of the nonlinear crystal, the phase delay may be different in the two direction of the polarization axes. The result is a polarization modulation. With the addition of polarizers at the input and output of the modulator, the change in the polarization leads to a variation of the amplitude of the output beam.

An alternative configuration, very common in fiber modulators and in integrated devices, employs this mechanism in a Mach–Zehnder interferometer. An input waveguide is split into two paths, i.e. the two arms of the interferometer, and then recombined into an output waveguide. The variable electric voltage is applied on one of these paths, resulting in an optical index modulation of one arm. The interference at the output waveguide builds the phase or intensity modulation of the beam.

Simplifying the model, the relation between the input and output beam power of an intensity modulator can be expressed as

$$I_{out} = \tau I_{in} \left[1 + \cos\left(\frac{\pi}{V_\pi} V + \Phi \right) \right] \tag{9.14}$$

where I_{in} is the input intensity, I_{out} is the output intensity, V_π is the half-wave voltage, that is the voltage required for inducing a phase change of π, and V is the modulation voltage. The coefficients τ and Φ describe a transmissivity and a phase term which take into account for losses and a mismatch between the two interferometer arms.

In the case of phase modulators, the phase variation obtained at the output is given by the affine equation

$$\phi = \frac{\pi}{V_\pi} V + \Phi \tag{9.15}$$

which involves the half-wave voltage V_π and the correction coefficient Φ.

Other type of modulators use analogous acousto-optical effects. Exploiting a piezoelectric transducer attached to the crystal, a sound wave is generated to provide a periodic refractive index grating. The traveling optical beam undergoes Bragg diffraction and propagates in a slightly different direction, enabling the possibility to build intensity (on–off) switching.

9.2.4 Photodetectors

While the other components of the optical transmission systems (laser, modulator and demodulator, transmitting and receiving antennas, and channel) have direct counterparts in a radiofrequency system, the detection in optical communications is performed almost exclusively by a photodetector, which is a very peculiar component of the optical technology, exploiting the photoelectric effect explained in quantum terms by Einstein in 1905.

The photodetection is the result of an interaction process between light and matter. Roughly speaking, a single photon in the optical beam releases an electron in the photosensitive material, which generates a pulse of electric current, converting optical power into an electric quantity. Before conversion, the electrons released by the photoelectric effect may be subjected to a multiplication procedure in which each electron generates a random number of secondary electrons.

From the classical point of view, the model may be the following. At the input, we get the instantaneous power

$$p(t) = \sum_k (h\nu)\, \delta(t - t_k)$$

where the instants t_k are the arrivals of a *doubly stochastic* Poisson process with intensity $\lambda(t)$ (see Fig. 4.28). The current produced by the photodetection can be modeled as a *filtered and marked Poisson process*, as discussed in Sects. 4.6 and 4.7, namely

$$i(t) = \sum_k g_k\, i_0(t - t_k), \tag{9.16}$$

where $i_0(t)$ is the current pulse generated by a single electrons satisfying the condition

$$\int_0^\infty i_0(t)\mathrm{d}t = e \tag{9.17}$$

with e electric charge of the electron. The coefficients g_k are independent and identically distributed random variables giving the number of electrons generated by the photon arrived at time t_k. They may take into account the random gain (if any) of the photomultiplication or the loss of photons in the material, caused by reflection and spreading, or both. In the first case the random variables g_i have mean $G > 1$, called the photomultiplication gain. In the second case g_k are binary random variable, whose mean η gives the photodetection efficiency.

The intensity $\lambda(t)$ of the Poisson process is proportional to the area A of the photodetector and to the intensity $J(t) = |\alpha(t)|^2$ of the electric field. In digital communications applications, $\lambda(t)$ turns out to be a random process, depending on the transmitted symbol. Then, the model of the photon arrivals is a doubly stochastic Poisson process.

Among practical impairments to the ideal behavior of the photodetectors, a role is played by the so-called dark current due to spontaneous emission of electrons in the photosensitive material. This is taken into account by a constant term λ_0 added to the useful intensity $\lambda(t)$.

In the decision process, the current (9.16) is integrated on the interval, say $(0, T]$, corresponding to a symbol slot, giving the quantity under decision

$$\mathcal{Q} = \int_0^T i(t)\mathrm{d}t = \sum_k^n g_k \int_0^T i_0(t - t_k)\mathrm{d}t = e\, n_T, \tag{9.18}$$

where n_T gives the electrons counting, i.e., the random number of electrons emitted in the slot symbol by the photodetector. The general statistics of n_T for a filtered and marked doubly stochastic Poisson process has been discussed in Chap. 4 (see also Fig. 4.28 for the detail of counting starting from the instantaneous power and current). On the value of the detected charge $\mathcal{Q}$, depending on the particular symbol transmitted, is based the decision process of the digital transmission scheme.

In the quantum communications applications the aim of the photodetector is limited in general to detect the presence of a positive number of photons in the optical beam, formulated as a quantum state $|\psi\rangle$. Thus a photodetector plays the role of counting the photons present in a given state $|\psi\rangle$ (Fig. 9.6). As discussed in Sect. 7.9.3, from a quantum point of view it must discriminate the vacuum state $|0\rangle$ from a coherent state

$$|\alpha\rangle = \mathrm{e}^{-|\alpha|^2/2} \sum_{n=0}^{\infty} \frac{\alpha^n}{\sqrt{n!}} |n\rangle. \tag{9.19}$$

The ideal quantum model of the detector reduces to a simple von Neumann measure with measurement operators (see (7.70))

$$Q_1 = \sum_{n=1}^{\infty} |n\rangle\langle n|\,, \qquad Q_0 = |0\rangle\langle 0| = I - Q_1 \tag{9.20}$$

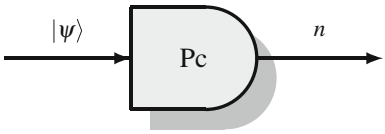

Fig. 9.6 Graphical symbol of a photon counter. The output n gives the number of photons present in the state $|\psi\rangle$

detecting 0 if and only the input state is $|0\rangle$. The resulting conditional probabilities are given by

$$p(0|0) = \langle 0|Q_0|0\rangle = 1\,, \qquad p(1|1) = \langle \alpha|Q_1|\alpha\rangle = 1 - \mathrm{e}^{-|\alpha|^2/2}. \tag{9.21}$$

If reduced efficiency and dark current are taken into account, the measurement operators becomes (see Problem 9.1)

$$Q_1 = \mathrm{e}^{-\mu} \sum_{n=0}^{\infty} (1-\eta)^n \, |n\rangle \, \langle n| \quad , \qquad Q_0 = I - Q_1 \tag{9.22}$$

where $\mu = \lambda_0 T$ is the average number of dark current electrons and η is the detection efficiency. The quantum state $|0\rangle$ is guessed if no dark electrons are present (with probability $\mathrm{e}^{-\mu}$) and, for any n , n photons are missed (with probability $(1-\eta)^n$). Note that in this case the measurement operators are POVM and not von Neumann projectors.

It must be noted that in any case the measurement performed by the photodetector is destructive in that, after the detection, the field is completely absorbed.

Problem 9.1 ⋆⋆ Consider the model of a photon counter where the dark current and the nonunitary efficiency are taken into account. Prove that the measurement operators are given by (9.22).

9.3 Classical Optical Communications Systems

9.3.1 Incoherent Detection

The simplest optical communication system uses amplitude modulation and incoherent detection (see Sect. 7.9). The transmitter associates a zero field to the binary symbol 0 and the field

$$v(t) = V_0 \cos 2\pi \nu t\,, \qquad 0 < t < T \tag{9.23}$$

to the binary symbol 1, where T is the symbol period. This is obtained by amplitude modulating the laser beam of frequency ν or, more simply, by switching on and off the laser itself according to the source symbol to be transmitted. At the receiver, a photodetector transforms the incident field into an electrical current, as discussed in Sect. 9.2.4.

In the absence of thermal noise, if the transmitted symbol is 0, the number of photons detected is zero; otherwise, it is a Poisson random variable n with mean value $\overline{n}$ proportional to V_0^2. An error may happen if and only if the symbol 1 is transmitted and the number of detected photons is 0. Then, the error probability turns out to be

$$P_e = \frac{1}{2}\mathrm{e}^{-\overline{n}} \tag{9.24}$$

where equally likely symbols are assumed. For the sake of comparison with other schemes it is convenient to express the error probability in terms of the *average number of photons per bit* N_R, given by $N_R = \frac{1}{2}\overline{n}$. Then

$$P_e = \frac{1}{2}\mathrm{e}^{-2\,N_R}. \tag{9.25}$$

The received scheme is called *direct detection* of the incident light pulses. The main advantage of this approach is its simplicity. In particular, phase and frequency instability of the laser source is well tolerated. Moreover, at the receiver direct detection is used and phase-sensitive devices are avoided.

This scheme, known as on–off keying (OOK) modulation, has a simple quantum equivalent, employing the coherent states $|0\rangle$ and $|\alpha\rangle$. As shown in Sect. 9.2.4, the photodetector can be modeled by a von Neumann measurement with projectors $Q_0 = |0\rangle\,\langle 0|$ e $Q_1 = I - |0\rangle\,\langle 0|$. The cross transition probabilities are

$$p(1|0) = \mathrm{Tr}[|0\rangle\,\langle 0|\,Q_1] = 0\,, \qquad p(0|1) = \mathrm{Tr}[|\alpha\rangle\langle\alpha|\,Q_0] = \mathrm{e}^{-|\alpha|^2} \tag{9.26}$$

so that the error probability becomes $P_e = \frac{1}{2}\mathrm{e}^{-|\alpha|^2}$. In terms of average number of photons per bit N_R, with equiprobable symbols one gets $N_R = |\alpha|^2/2$, so that we find again

$$P_e = \frac{1}{2}\mathrm{e}^{-2N_R}. \tag{9.27}$$

This result is known as the **quantum limit** (or **shot noise limit**) and is the optimum for any detection that does not exploit the coherence property of the optical beam.

9.3.2 Coherent Homodyne Detection

A more sophisticated scheme of classical optical communication uses binary phase shift keying (BPSK) modulation (see Sect. 7.10.2). The laser beam is applied to a π-phase modulator driven by the binary symbol source. As a consequence, the optical field at the receiver assumes one of the values

$$v(t) = V_0\,\cos(2\pi\,\nu t + A_0\pi) \tag{9.28}$$

depending on the source symbol $A_0 \in \mathcal{A} = \{0, 1\}$.

Since the signals for different symbols have the same optical energy, direct detection cannot discriminate between them. In the coherent homodyne detection scheme the receiver sums to the field a high level field $V_L \cos 2\pi\,\nu t$ with the same frequency

as $v(t)$ but with larger amplitude ($V_L \gg V_0$) generated by a local laser. The global field

$$V_0 \cos(2\pi \nu t + A_0 \pi) + V_L \cos 2\pi \nu t = (V_0 \cos A_0 \pi + V_L) \cos 2\pi \nu t \tag{9.29}$$

applied to a photodetector produces a number of electrons which is a Poisson random variable with mean and variance proportional to

$$V_L^2 + V_0^2 + 2 \cos A_0 \pi \; V_0 V_L = V_L^2 + V_0^2 + 2 B_0 \, V_0 V_L \tag{9.30}$$

where

$$B_0 = \cos A_0 \pi = \begin{cases} +1 & A_0 = 0 \\ -1 & A_0 = 1. \end{cases} \tag{9.30a}$$

Then, having subtracted the bias term $V_L^2 + V_0^2$ independent of the symbol, one obtains the useful signal proportional to $2 B_0 V_0 V_L$. As the amplitude V_L of the local laser field increases, an approximate Gaussian characterization of signal and noise may be adopted, so that the receiver must discriminate between two signal proportional to $2 B_0 V_0 V_L$ with Gaussian noise having variance

$$\sqrt{V_L^2 + V_0^2 + 2 B_0 V_0 V_L} \approx V_L. \tag{9.31}$$

This can be obtained by a threshold decision device [2], that is, a device which sets a threshold and estimates the received symbol depending on whether the measured signal is above or below such a threshold. With equiprobable symbols the optimal threshold is 0 and the error probability becomes (see homodyne receiver in Sect. 7.10.2)

$$P_e = Q(2V_0) = Q(\sqrt{4N_R}), \tag{9.32}$$

where $Q(x)$ is the Gaussian complementary distribution and N_R is the average number of photons per bit. This error probability is known as the **standard quantum limit**.

Comparison with incoherent detection shows that the performances of the homodyne detection are largely better. On the other hand the implementation of an efficient homodyne scheme implies some complications, in that it requires the presence of a local laser that must be accurately tuned in frequency and phase with the source laser.

9.4 Binary Quantum Communications Systems

The simplest quantum communication systems use binary schemes in which Alice associates to the symbol A_0 of a classical binary source, $A_0 \in \{0, 1\}$, with prior probabilities q_0 and q_1, two coherent quantum states $|\gamma_0\rangle$ and $|\gamma_1\rangle$ and Bob performs

a measurement on the system by using two measurement operators Q_0 and Q_1. The most common choices are $|\gamma_0\rangle = |0\rangle$ and $|\gamma_1\rangle = |\beta\rangle$ for the On–Off Keying (OOK) scheme (see Fig. 7.22) and $|\gamma_0\rangle = |-\beta\rangle$ and $|\gamma_1\rangle = |\beta\rangle$ for the Binary Phase Shift Keying (BPSK) scheme (see Fig. 7.25).

For the sake of comparison with practical systems we begin by reviewing the ideal detection approach leading to the Helstrom bound. Next we consider in detail the OOK with direct detection and the BPSK with Kennedy's detection. Particular attention will be given to the Dolinar's receiver which promises to achieve the optimum performance, i.e., the Helstrom bound.

9.4.1 Recall of Helstrom's Theory

We reconsider the general theory of binary detection developed in Sect. 5.4.2 according to the geometric approach. The state vectors are written in terms of an appropriate orthonormal basis $\{|u_0\rangle, |u_1\rangle\}$ as

$$|\gamma_0\rangle = \cos\theta|u_0\rangle + \sin\theta|u_1\rangle\,, \qquad |\gamma_1\rangle = \cos\theta|u_0\rangle - \sin\theta|u_1\rangle \tag{9.33}$$

where $\cos 2\theta = \langle\gamma_0|\gamma_1\rangle = X$ is the superposition coefficient assumed to be real. The orthonormal measurement vectors are written as

$$|\mu_0\rangle = \cos\phi|u_0\rangle + \sin\phi|u_1\rangle\,, \qquad |\mu_1\rangle = -\sin\phi|u_0\rangle + \cos\phi|u_1\rangle. \tag{9.34}$$

Then the transition probabilities $p(j|i) := P[\hat{A}_0 = j|A_0 = i]$ are given by

$$p(0|0) = \cos^2(\phi - \theta)\,, \qquad p(1|1) = \sin^2(\phi + \theta) \tag{9.35}$$

and the correct detection probability turns out to be

$$P_c = q_0|\langle\mu_0|\gamma_0\rangle|^2 + q_1|\langle\mu_1|\gamma_1\rangle|^2 = q_0\cos^2(\phi - \theta) + q_1\sin^2(\phi + \theta). \tag{9.36}$$

Here the angle θ is given through the superposition coefficient X, while the angle ϕ is unknown and is evaluated by optimization. We have seen that the angle ϕ giving the maximum of P_c satisfies the conditions

$$\sin 2\phi = \frac{1}{R}\sin 2\phi \quad , \qquad \cos 2\phi = \frac{q_0 - q_1}{R}\cos 2\theta \tag{9.37}$$

where $R = \sqrt{1 - 4q_0q_1X^2}$. The corresponding optimal correct decision probability is

$$P_c = \frac{1}{2}(1+R) = \frac{1}{2}\left(1+\sqrt{1-4q_0q_1X^2}\right), \tag{9.38}$$

i.e., the Helstrom bound.

We have also seen (see Problem 7.10) that the **a posteriori probabilities** $q(i|j) := \mathrm{P}[A_0 = i|\hat{A}_0 = j]$ corresponding to the optimal decision are related to the correct decision probability by

$$q(0|0) = q(1|1) = P_c. \tag{9.39}$$

In other words, the measurement modifies the a priori probabilities in the sense that, independently of the measurement result, the symbol guessed acquires a posteriori probability coinciding with the probability of correct decision.

Finally, we note that the measurement vectors are entangled linear combinations of the state vectors. Unfortunately, since in practice only photodetectors and phase-sensitive devices are available, the optimal measurement vectors are very hard to be implemented experimentally. So, for a long time suboptimal approaches have been investigated and experimented and only recently experiments demonstrating the feasibility of the optimal measurement have been accomplished.

9.4.2 Kennedy's Receiver

In 1973 Kennedy [3] proposed a very simple quantum receiver for the Binary Phase Shift Keying (BPSK). The received quantum state ($|\beta\rangle$ or $|-\beta\rangle$) is applied to one of the inputs of a beam splitter with high transmissivity τ. To the other input of the beam splitter a quantum state $|\beta\rangle$ is applied, produced by a local laser tuned in frequency and phase with the laser of the transmitter. The corresponding displacement $D(\beta)$ changes the possible input states into $|\gamma_0\rangle = |0\rangle$ and $|\gamma_1\rangle = |2\beta\rangle$, according to an approach called **nulling technique**. Then, as in the OOK receiver, one applies to the displaced state the photodetection with measurement projectors $P_0 = |0\rangle\langle 0|$ and $P_1 = 1 - P_0$. The resulting error probability turns out to be

$$P_e = q_1 \mathrm{Tr}(|\gamma_1\rangle\langle\gamma_1| P_0) = q_1 \mathrm{e}^{-4|\beta|^2}, \tag{9.40}$$

or, with equally likely symbols and in terms of the average number of photons per bit

$$P_e = \frac{1}{2}\mathrm{e}^{-4N_R}. \tag{9.41}$$

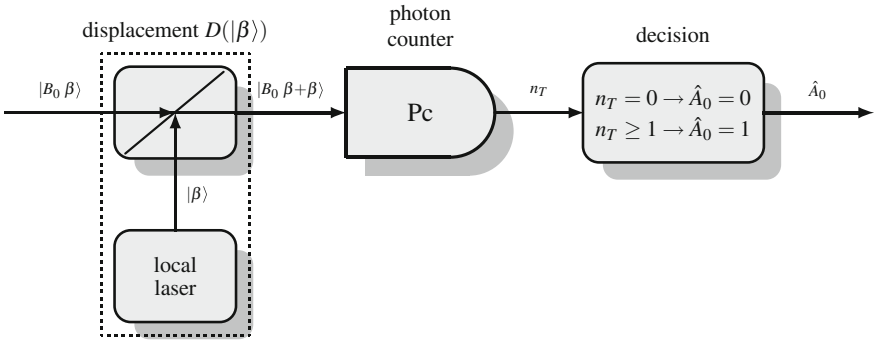

Fig. 9.7 Scheme of Kennedy's receiver. The displacement is obtained with a beam splitter feeded by the received state $|B_0\ \beta\rangle$ and the state $|\beta\rangle$ produced by a local laser. The received state takes one of the two values $|\pm\beta\rangle$ and, after the displacement, the values $|0\rangle$ and $|2\beta\rangle$, respectively. B_0 is the binary symbol $B_0 = \cos A_0\pi = \begin{cases} +1 & A_0 = 0 \\ -1 & A_0 = 1 \end{cases}$

The transmitter uses a π phase modulator driven by the input symbol. The receiver uses a local laser generating the coherent state $|\beta\rangle$ to be added to the input coherent state by a beam splitter realizing the displacement $D(\alpha)$. The scheme of the system is depicted in Fig. 9.7.

The feasibility of the Kennedy receiver has been demonstrated (see f.i. [4]). The main difficulties in the implementation are related to the presence of two lasers, the source laser and the local one, whose frequencies, phases, and levels must be accurately tuned. As a matter of fact, most practical demonstrations use a single laser source from which both the optical beam and the local beam simulating the useful carrier are derived through a beam splitter.

The performance of the Kennedy's receiver is presented in Fig. 9.8 in comparison with the performance of the OOK scheme and Helstrom's bound. The relations used are

$$\begin{aligned} P_{e,\mathrm{OOK}} &= \tfrac{1}{2}\,\mathrm{e}^{-N_R} \\ P_{e,\mathrm{Kennedy}} &= \tfrac{1}{2}\,\mathrm{e}^{-4N_R} \\ P_{e,\mathrm{Helstrom}} &= \tfrac{1}{2}\left[1 - \sqrt{1 - \mathrm{e}^{-4N_R}}\right] \end{aligned}$$

where N_R is the average number of photons per bit. The error probability plotted versus N_R shows that the Kennedy's receiver outperforms the OOK direct receiver, but is overperformed by the Helstrom's bound.

On the other hand, the Kennedy receiver does not outperforms the standard quantum limit of the homodyne detection for week signals ($N_R < 0.4$). But also for greater values of the number N_R of the received photons the performance of Kennedy's

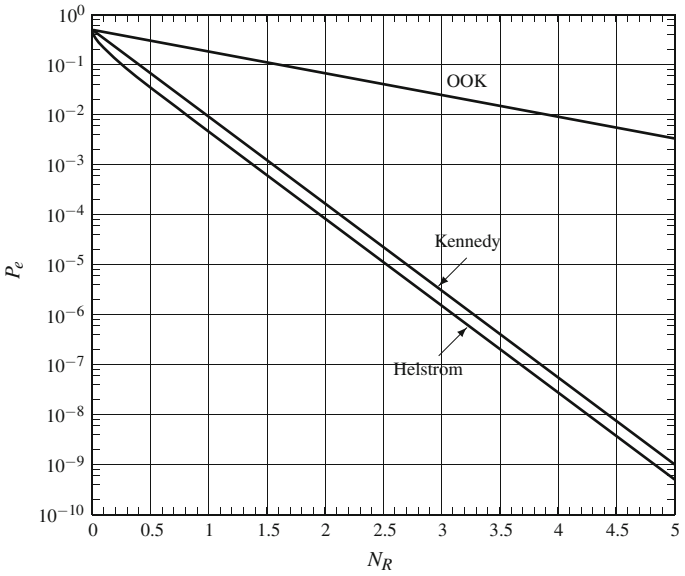

Fig. 9.8 Comparison of OOK, Kennedy's receiver, and Helstrom's bound in terms of error probability versus the average number of photons N_R

receiver in practical experiments is inferior to the standard quantum limits. Indeed, impairments of the photodetector, as reduced quantum efficiency and dark current, has relevant negative effects on the error probability [5].

9.4.3 Improved Kennedy's Receiver

Improvements to Kennedy's receiver have been suggested in recent years by Takeoka and Sasaki [5]. The basic idea is to apply to the input state a displacement $|\varepsilon\rangle$ with ε chosen in such a way that the error probability is minimized. The quantum states $|\beta\rangle$ and $|-\beta\rangle$ are displaced into the states $|\gamma_1\rangle = |\varepsilon + \beta\rangle$ and $|\gamma_0\rangle = |\varepsilon - \beta\rangle$. The error probability becomes

$$\begin{aligned} P_e &= q_1 \mathrm{Tr}(|\gamma_1\rangle \langle\gamma_1| \, P_0) + q_0 \mathrm{Tr}(|\gamma_0\rangle \langle\gamma_0| \, P_1) \\ &= q_1 \mathrm{e}^{-(\varepsilon+\beta)^2} + q_0 (1 - \mathrm{e}^{-(\varepsilon-\beta)^2}). \end{aligned} \tag{9.42}$$

(For the sake of simplicity we assume that β and ε are real). By nulling the derivative with respect to ε, we find that the displacement ε_0 minimizing P_e satisfies the transcendental equation

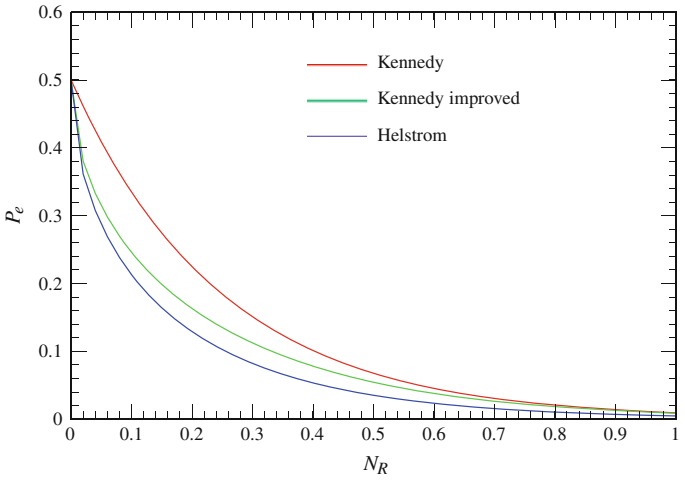

Fig. 9.9 Comparison of Kennedy's receiver, improved Kennedy's receiver, and Helstrom's bound in terms of error probability versus the average number of photons N_R

$$\frac{q_1}{q_0} = \frac{\varepsilon - \beta}{\varepsilon + \beta} \mathrm{e}^{4\beta\varepsilon}. \tag{9.43}$$

In Fig. 9.9 the performance of the Kennedy receiver and of the improved Kennedy receiver are compared with the Helstrom bound. The relations used are

$$P_{e,\text{Kennedy}} = \tfrac{1}{2}\, \mathrm{e}^{-4N_R}$$
$$P_{e,\text{Kennedy improved}} = \tfrac{1}{2}\left[1 + \mathrm{e}^{-(\varepsilon_0+\sqrt{N_R})} - \mathrm{e}^{-(\varepsilon_0-\sqrt{N_R})}\right]$$
$$P_{e,\text{Helstrom}} = \tfrac{1}{2}\left[1 - \sqrt{1 - \mathrm{e}^{-4N_R}}\right]$$

where $N_R = \beta^2$ is the average number of photons per bit. For large values of β, the improvement obtained by optimizing the displacement ε appears to be negligible. On the other hand, as β goes to 0, the improved Kennedy's receiver approximates the Helstrom's bound very well and outperforms the standard quantum limit also for weak signals. This has an important consequence in the interpretation of the optimum Dolinar's receiver. The feasibility of the improved Kennedy's receiver has been recently demonstrated by Wittmann et al. [6].

Further light improvements [5] can be obtained if the input state is subjected to a displacement $D(\varepsilon)$ and to a squeezing $Z(r)$ (to be jointly optimized) before the photodetection.

9.4.4 Dolinar's Receiver

In 1973 Dolinar [7] proposed an adaptive measurement scheme, based on a combination of photon counting and feedback control, that precisely achieves the Helstrom bound. However, since the scheme requires a very precise control of an optical–electrical loop, only in 2007 Dolinar's idea has obtained a satisfactory practical implementation [4, 8].

In order to give some insight on Dolinar's approach, we consider the problem of discriminating between the states given by multiple copies

$$|\alpha_0\rangle = |\alpha\rangle \otimes \cdots \otimes |\alpha\rangle \quad , \quad |\alpha_1\rangle = |-\alpha\rangle \otimes \cdots \otimes |-\alpha\rangle \tag{9.44}$$

in the tensorial product Hilbert space $\mathcal{H}^{\otimes n}$ where $\mathcal{H}$ is the Hilbert space spanned by the single copies $|\alpha\rangle$ and $|-\alpha\rangle$. Of course, Helstrom's theory assures that the optimum receiver gives the Helstrom's bound

$$P_c^{(n)} = \frac{1}{2}\left(1 + \sqrt{1 - 4q_0 q_1 X^{2n}}\right), \tag{9.45}$$

with $X = |\langle\alpha|-\alpha\rangle|$, so that $|\langle\alpha_0|\alpha_1\rangle| = X^n$. On the other hand, the optimal measurement vectors in $\mathcal{H}^{\otimes n}$ derived according to the Helstrom's theory are entangled vectors difficult to be realized experimentally. However, Acin et al. [9] have shown that the optimum can be achieved by adaptive local measurements on the single copies, each one taking into account the results of the previous measurements (for greater details see [10]).

Confining ourselves to the case $n = 2$, assume that the optimum measurement has been performed on the first state with correct decision probability $P_c^{(1)}$ given by (9.45) with $n = 1$. Moreover, assume that as a consequence of the measurement state $|\alpha\rangle$ has been guessed. Then, as discussed above, the a posteriori probabilities of $|\alpha\rangle$ and $|-\alpha\rangle$ become $q_0' = P_c^{(1)}$ and $q_1' = 1 - P_c^{(1)}$. If we perform an optimum measurement on the second state on the basis of the probabilities q_1' and q_0' and with corresponding new measurement vector, after the measurement we get the correct result with probability

$$P_c^{(2)} = \frac{1}{2}\left(1 + \sqrt{1 - 4(1 - P_c^{(1)})P_c^{(1)}X^2}\right) = \frac{1}{2}\left(1 + \sqrt{1 - 4q_0 q_1 X^4}\right). \tag{9.46}$$

The same result is obtained if the state guessed after the first measurement is $|-\alpha\rangle$. By iterating the reasoning, the result can be generalized to n-copies states. The process can be considered as a feedback-assisted detection, in that the measurement on each copy is chosen on the basis of the result of the previous measurements.

These considerations can be applied to BPSK coherent states $|\beta\rangle$ and $|-\beta\rangle$ when they correspond to wavepackets having temporal extent of duration T. In this case, the mode can be thought as a sequence of shorter and weaker modes of duration T/n, namely,

$$|\beta\rangle = \left|\frac{\beta}{\sqrt{n}}\right\rangle \otimes \cdots \otimes \left|\frac{\beta}{\sqrt{n}}\right\rangle \tag{9.47}$$

with an analogous decomposition for $|-\beta\rangle$. Moreover, as n increases and the average number of photons per copy goes to zero, as shown above, the optimal Helstrom measurement on each copy may be conveniently approximated by an improved Kennedy receiver, i.e., a displacement followed by a photon detection.

The multiple-copy approach discussed above is mimicked by the Dolinar's receiver. Let be

$$\psi(t) = \pm\psi e^{i2\pi\nu t}, \qquad 0 \le t \le T \tag{9.48}$$

the input fields corresponding to the coherent states $|\pm\beta\rangle$. At the detector from the input field a time-varying field generated by a local laser is subtracted. The envelope of this local field is chosen between either $u_0(t)$ or $u_1(t)$, accordingly to the value of $z(t)$, a binary signal with possible values 0 and 1, giving the provisional decision at time t. Then, depending on the value of $z(t)$, the optical signal at the photon counter has enveloped either $\pm\psi - u_0(t)$ or $\pm\psi - u_1(t)$. The decision signal $z(t)$ is assumed changing at any photon arrival at the counter.

The mathematical problem is to choose the functions $u_0(t)$ and $u_1(t)$ that maximize the correct detection probability $\mathrm{P}[z(T) = a]$, where a is the source symbol and $z(T)$ is the final decision. The problem has been solved by Geremia [11] on the basis of the dynamic programming optimality principle.

A simpler proof based on a semiclassical analysis given by Assalini et al. [10] is sketched here, under the preliminary assumption that the subtracted envelopes are opposite, namely $u_1(t) = -u_0(t)$. Provided that the transmitted symbol is $a = 0$ and consequently the received envelope is β, the process $z(t)$ can be interpreted as a telegraph process [12] alternately driven by non-homogeneous Poisson processes with rates

$$\lambda(t) = |\beta - u_0(t)|^2 \quad , \qquad \mu(t) = |\beta + u_0(t)|^2. \tag{9.49}$$

Defined the conditional probability $p_0(t) = \mathrm{P}[z(t) = 0|a = 0]$ and $N_{t,\Delta t}$ the number of arrivals in the interval $[t, t + \Delta t)$

$$\begin{aligned} p_0(t+\Delta) &= \mathrm{P}[z(t) = 0, N_{t,\Delta t} = 0|a = 0] + \mathrm{P}[z(t) = 1, N_{t,\Delta t} = 1|a = 0] + \mathrm{o}(\Delta t) \\ &= \mathrm{P}[N_{t,\Delta t} = 0|z(t) = 0]p_0(t) + \mathrm{P}[N_{t,\Delta t} = 1|z(t) = 1](1 - p_0(t)) + \mathrm{o}(\Delta t) \\ &= [\,1 - \lambda(t)\Delta t\,]p_0(t) + \mu(t)\Delta t(1 - p_0(0)) + \mathrm{o}(\Delta t). \end{aligned}$$

Hence the differential equation

$$p_0'(t) = \mu(t) - [\,\lambda(t) + \mu(t)\,]p_0(t) \tag{9.50}$$

follows. In a similar way can be shown that $p_1(t) = \mathrm{P}[z(t) = 1|a = 1]$ satisfies the same differential equation, so that the probability of correct decision satisfies the differential equation

$$P_c'(t) = q_0 p_0'(t) + q_1 p_1'(t) = \mu(t) - [\,\lambda(t) + \mu(t)\,]P_c(t) \tag{9.51}$$

independent of the symbol probabilities q_0 and q_1. If we impose

$$P_c(t) = \frac{1}{2}\left[1 + \sqrt{1 - 4q_0 q_1 \mathrm{e}^{-4\beta^2 t}}\right] \tag{9.52}$$

coinciding with Helstrom's bound, a simple algebra shows that the differential equation is satisfied by setting

$$u_0(t) = \frac{\beta}{\sqrt{1 - 4q_0 q_1 \mathrm{e}^{-4\beta^2 t}}} \quad , \qquad 0 < t < T\,. \tag{9.53}$$

This gives the control optical signal achieving Dolinar's bound.

A conceptual scheme of Dolinar's receiver is depicted in Fig. 9.10. An amplitude-modulated local laser produces the optical beam with complex envelope $u_0(t)$ to be added or subtracted to the input beam. The choice between $\pm u_0(t)$ is performed by

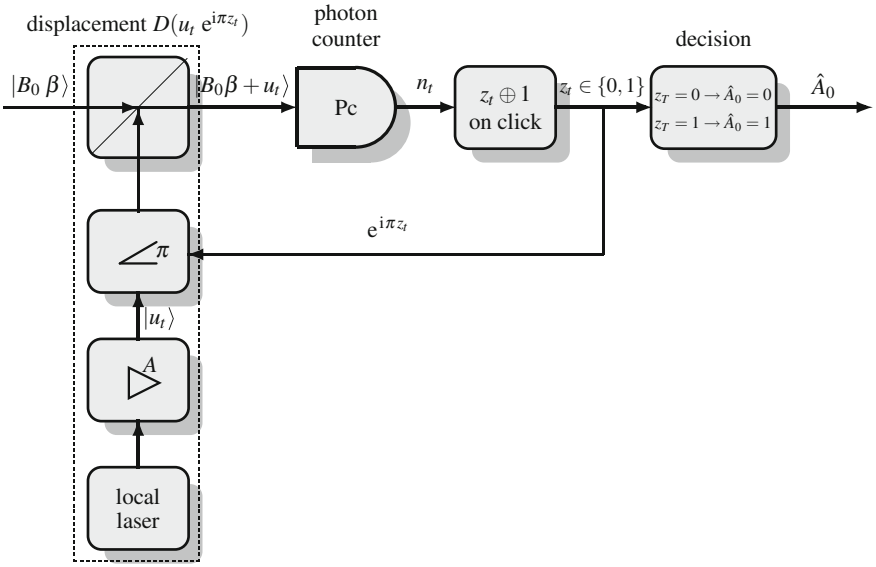

Fig. 9.10 Scheme of Dolinar's receiver: note that $z_t \oplus 1$ represents a change of 0 and 1 at every click. z_t represents the provisional symbol estimation. At the end of the symbol period, the final decision z_T is taken

a π phase modulator driven through a feedback control by the photon arrivals at the photodetector.

Of course the problems of tuning in frequency and phase the lasers encountered in Kennedy's receiver stay on. Another difficulty arises in amplitude modulating the local laser in such a way that the local envelope (9.53) is obtained. Finally, the unavoidable delays introduced by the optical–electrical feedback control may greatly reduce the performance of the system. As a consequence, the implementation of the optimal receiver out of the laboratories appears to be at present a very difficult task.

9.4.5 The Sasaki–Hirota Receiver

Sasaki and Hirota have shown [13] that in principle it is possible to achieve the Helstrom bound by considering the problem in the two-dimensional Hilbert space spanned by the states $|-\alpha\rangle$ and $|\alpha\rangle$.

Since to the input state it may be applied a displacement $|\alpha\rangle$ as in the Kennedy receiver, we may consider as input states $|0\rangle$ and $|2\alpha\rangle$. It may be easily verified that the states

$$|\eta_1\rangle = |0\rangle \quad , \qquad |\eta_2\rangle = \frac{1}{\sqrt{1-X^2}}(|2\alpha\rangle - X|0\rangle) \tag{9.54}$$

with $X = \langle 0|2\alpha\rangle$ (α is assumed to be real) form an orthonormal basis of the Hilbert space $\mathcal{H}_0$ spanned by $|0\rangle$ and $|2\alpha\rangle$. Then, consider the operator

$$U(\theta) = \cos\theta(|\eta_1\rangle\langle\eta_1| + |\eta_2\rangle\langle\eta_2|) + \sin\theta(|\eta_1\rangle\langle\eta_2| - |\eta_2\rangle\langle\eta_1|). \tag{9.55}$$

A simple algebra shows that $U(\theta)U^*(\theta) = |\eta_1\rangle\langle\eta_1| + |\eta_2\rangle\langle\eta_2|$ coincides with the identity operator in $\mathcal{H}_0$, so that $U(\theta)$ is a unitary operator in $\mathcal{H}_0$. The Sasaki–Hirota approach assumes that the unitary operator $U(\theta)$ is applied to the displaced state ($|0\rangle$ or $|2\alpha\rangle$) and that the transformed state is subjected to a von Neumann measurement with projectors

$$Q_1 = |\eta_1\rangle\langle\eta_1| \, , \qquad Q_2 = |\eta_2\rangle\langle\eta_2| \, . \tag{9.56}$$

If the error probability is computed and optimized with respect to the angle θ, the Helstrom bound is achieved. For greater mathematical details see [11, 13].

Note that, while the measurement state $|\eta_1\rangle = |0\rangle$ is a coherent state, $|\eta_2\rangle$ is not. On the other hand, since $\langle 0|\eta_2\rangle = 0$, it is innocuously substitutes the measurement operator $|\eta_2\rangle\langle\eta_2|$ with

$$\sum_{n=1}^{\infty} |n\rangle\langle n| \tag{9.57}$$

and the detection may be realized in the Glauber space with an ideal photodetector. On the contrary, the unitary operator $U(\theta)$ is not Gaussian (see Chap. 11), so that it is not realizable with usual linear optics and requires nonlinear unpractical components [13].

9.5 Multilevel Quantum Communications Systems

In spite of the fact that K-ary quantum systems can in principle achieve greater capacity than binary systems, only recently attention has been paid to implementable receivers for K-ary quantum communications with $K > 2$. Indeed, simple modulations as K-PSQ, QAM, and PPM have been frequently considered from a theoretical point of view but practical receivers are very difficult to be realized. In this section, we present some recent ideas concerning possible suboptimal receivers, in particular for K-PSK and PPM quantum systems.

9.5.1 Multiple PSK and QAM Quantum Systems

The coherent states of a K-PSK constellation are

$$|\alpha_k\rangle = |\alpha_0 \mathrm{e}^{i2\pi k/K}\rangle\,, \qquad k = 0, \ldots, K-1 \tag{9.58}$$

and may be written as $|\alpha_k\rangle = S^k|\alpha_0\rangle$ with $S = \mathrm{e}^{i2\pi N/K}$, where N is the number operator (see Sect. 7.12.1). As shown above (see also [14]), this constellation enjoys geometrical uniform symmetry so that the SRM derived by the Gram matrix is optimal. However, the optimal measurement vectors turn to be entangled and difficult to realize. Similar considerations hold for QAM systems.

In [15], a suboptimal receiver for K-ary quantum systems is suggested based on suitable combinations of beam splitters, displacements, and photodetectors and following the ideas lying behind the Kennedy and Kennedy-improved detectors. Since the extensions to $K > 3$ appear intuitive, we confine ourselves to the case $K = 3$ (with possible states $|\alpha_0\rangle$, $|\alpha_1\rangle$ and $|\alpha_2\rangle$) and follow the scheme of Fig. 9.11. The input state is applied to a beam splitter with transmissivity τ. The first output of the beam splitter is displaced by a displacement $D(-\sqrt{1-\tau}\alpha_0)$, the second one by a displacement $D(-\sqrt{\tau}\alpha_1)$. The displaced states enter two photodetectors. Provided that the input state is $|\alpha_i\rangle$, the outputs of the beam splitter are given by$|b_1\rangle = |\sqrt{1-\tau}\alpha_i\rangle$ and $|b_2\rangle = |\sqrt{\tau}\alpha_i\rangle$ and the output of the displacements are $|c_1\rangle = |\sqrt{1-\tau}(\alpha_i - \alpha_0\rangle$ and $|c_2\rangle = |\sqrt{\tau}(\alpha_i - \alpha_1\rangle$. In conclusion, we have the following states in correspondence with the possible input state

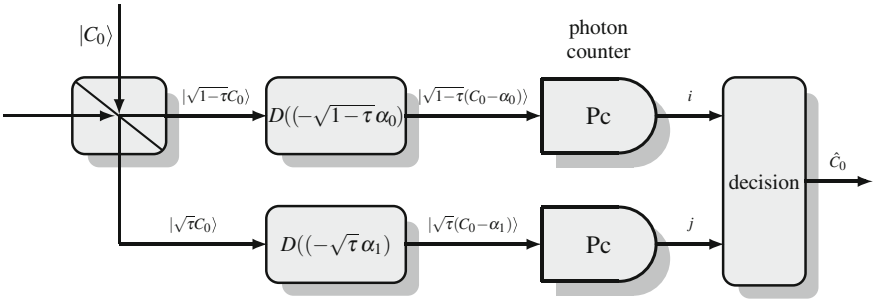

Fig. 9.11 Scheme of a ternary quantum system. C_0 is the transmitted complex (random) symbol and $|C_0\rangle$ the corresponding quantum state

$$\begin{aligned} |\alpha_0\rangle &\rightarrow |0\rangle \otimes |\sqrt{\tau}(\alpha_0-\alpha_1)\rangle \\ |\alpha_1\rangle &\rightarrow |\sqrt{1-\tau}(\alpha_1-\alpha_0)\rangle \otimes |0\rangle \\ |\alpha_2\rangle &\rightarrow |\sqrt{1-\tau}(\alpha_2-\alpha_0)\rangle \otimes |\sqrt{\tau}(\alpha_2-\alpha_1)\rangle. \end{aligned} \tag{9.59}$$

Denoting by (i, j), $i, j \in \{0, 1\}$ the output of the photodetectors, the transition probabilities $p(i, j|\alpha_k)$ can be computed. For instance, if the input state is $|\alpha_1\rangle$, the probability that the first detector does not detect photons is $\mathrm{e}^{-(1-\tau)|\alpha_1-\alpha_0|^2}$, while the probability that the second detectors does not detect photons is 1, so that

$$p(0, 0|\alpha_1) = \mathrm{e}^{-(1-\tau)|\alpha_1-\alpha_0|^2}.$$

On the basis of the transition probabilities, one computes the optimum decision rule minimizing the error probability. Of course, this error probability depends on the transmissivity τ. Then a second optimization with respect to τ may be performed. The resulting error probability outperforms the standard quantum limit. Better performances can be achieved if, as in the improved Kennedy receiver, the nulling displacements $|-\alpha_0\rangle$ and $|-\alpha_1\rangle$ are substituted by optimized displacements [15].

Further improvements are possible by suitably squeezing the signals after the displacements [16].

9.5.2 Pulse Position Modulation Systems

A quantum modulation scheme that enjoys large popularity owing to its simplicity is the pulse position modulation (PPM) scheme. In this scheme, a K-ary classical symbol with alphabet $\{0, \ldots, K-1\}$ is encoded into the position of a coherent state $|\alpha\rangle$ in a sequence of $K-1$ null states. The natural environment for such modulation is the tensor Hilbert space $\mathcal{H}_0^{\otimes K}$, where $\mathcal{H}_0$ is the Fock space. The possible states are the tensor states

$$|\alpha_0\rangle = |\alpha\rangle \otimes |0\rangle \otimes \cdots \otimes |0\rangle \qquad \cdots \qquad |\alpha_{K-1}\rangle = |0\rangle \otimes |0\rangle \otimes \cdots \otimes |\alpha\rangle.$$

The corresponding modulation technique is very simple and requires only the switching of the source laser.

The symmetry of the constellation is clear, even though it is by no means trivial to evaluate the symmetry operator in the Hilbert space $\mathcal{H}_0^{\otimes K}$ [17]. The optimal error probability (see Sect. 7.12.4) turns out to be

$$P_e = \frac{K-1}{K^2}\left(\sqrt{1+(K-1)p} + \sqrt{1-p}\right)^2 \tag{9.60}$$

where $p = \mathrm{e}^{-|\alpha|^2}$ is the probability that the state $|\alpha\rangle$ is not detected. The optimal measurement, coinciding with the SRM, enjoys the same symmetry of the states but is strongly entangled and appears very difficult to implement.

Note that in the K-PPM scheme each of the K symbols is carried by a state with average number of photons given by $|\alpha|^2$. The number of photons per bit is given bt $N_R = |\alpha|^2/\log_2 K$ and the error probability in terms of number of photons per bit is given by (9.60) with

$$p = \mathrm{e}^{-N_R \log_2 K}.$$

Several suboptimal measurements have been proposed. The simplest idea is to measure the single pulses with direct detection. In the absence of impairments in the photodetector, the error happens only when the single nonzero state is not detected, so that, guessing at random the symbol, the error probability is

$$P_e = \frac{K-1}{K}p.$$

A more sophisticated approach [18], known as *conditionally nulling receiver*, uses the following adaptive decision strategy. During the first signaling slot, a nulling state $|-\alpha\rangle$ is added. If the photodetector does not detect a photon, one provisionally decides for $|\alpha_0\rangle$, then the photodetection continues without nulling and the decision is maintained unless some photon is detected in the subsequent slots. If some photon is detected in the first interval, the hypothesis $|\alpha_0\rangle$ is discarded and the procedure is iterated. The error probability is computed recursively. For $K = 2$, one gets $P_{\mathrm{e}}^{(2)} = p^2/2$ because error occurs if and only if the state is $|\alpha_1\rangle$ and two pulses are undetected. For $K > 2$, no error occurs if the state is $|\alpha_0\rangle$, whereas in any other case (with probability $K/(K-1)$) error may occur if the nulling pulse in the first slot and the subsequent pulse are missed or if the nulling pulse is detected and an error happens in the remaining $K-1$ slots. In conclusion, the recursive relation

$$P_e^{(K)} = \frac{K-1}{K}[\, p^2 + (1-p)P_{\mathrm{e}}^{(K-1)}]$$

follows. In closed form one gets [19]

$$P_e^{(K)} = \frac{1}{K}[(1-p)^K - 1 + Kp].$$

Slight performance improvements are obtained applying a nonexact (and optimized) nulling pulse as in the improved Kennedy's receiver [20]. The algorithm of the conditionally nulling receiver is mimicked applying a constant displacement $D(\varepsilon)$ with $\varepsilon \neq -\alpha$ in place of the nulling operation. A numerical optimization of the value of the displacement shows an improvements in the performance, as demonstrated in the experimental test reported in [21].

Further performance enhancements can be obtained by considering different displacement ε_i in place of the nulling operations in the slots $i = 0, \ldots, M-1$, which in general may depend on all the outcomes in the previous measurements, rather than only the last o ne.

The general structure of such a receiver is an *adaptive* scheme with local measurement in each Fock space $\mathcal{H}_0$ optimized upon all the previous outcome. Each local measurement implements a binary discrimination between the ground state $|0\rangle$ and the coherent state $|\alpha\rangle$, which may be performed with direct detection, Kennedy or Dolinar schemes depending on the design limitations or constraints.

Due to the binary outcome of each local measurement, the overall receiver strategy can be described with a binary tree, where each node corresponds to a measurement and each edge to an outcome. The binary tree is covered from the root node to the final one following the path dictated by the outcomes, performing the measurement defined in the node that come across.

Since the total number of the measurement employed grows exponentially in the cardinality K of the alphabet, a global optimization of the measurement parameter may be really demanding. However, the required numerical optimization may be lightened using a dynamic programming approach [22].

The adaptive receiver shows an improvement in the performance due to the greater flexibility of the binary discrimination scheme employed and the more general measurement sequencing, which may depend upon all the previous partial outcomes. The improvement is seen for all the alphabet cardinalities K, and in particular for $K = 2$ this receiver precisely reaches the Helstrom bound of the error probability [22].

References

1. A.E. Siegman, *Lasers* (University Science Book, Sausalito, 1986)
2. C.W. Helstrom, Quantum detection and estimation theory. *Mathematics in Science and Engineering* (Academic Press, New York, 1976)
3. R.S. Kennedy, A near-optimum receiver for the binary coherent state quantum channel. Massachusetts Institute of Technology, Cambridge (MA), Technical Report January 1973, MIT Research Laboratory of Electronics Quarterly Progress Report 108

4. C.W. Lau, V.A. Vilnrotter, S. Dolinar, J. Geremia, H. Mabuchi, Binary quantum receiver concept demonstration. NASA, Technical Report, 2006, Interplanetary Network Progress (IPN) Progress Report 42–146
5. M. Takeoka, M. Sasaki, Discrimination of the binary coherent signal: Gaussian-operation limit and simple non-Gaussian near-optimal receivers. Phys. Rev. A **78**, paper no. 022320 (2008)
6. C. Wittmann, M. Takeoka, K.N. Cassemiro, M. Sasaki, G. Leuchs, U.L. Andersen, Demonstration of near-optimal discrimination of optical coherent states. Phys. Rev. Lett. **101**, paper no. 210501 (2008)
7. S.J. Dolinar, An optimum receiver for the binary coherent state quantum channel, Massachusetts Institute of Technology, Cambridge (MA), Technical Report, October 1973, MIT Research Laboratory of Electronics, Quarterly Progress Report 111
8. R.L. Cook, P.J. Martin, J.M. Geremia, Optical coherent state discrimination using a closed-loop quantum measurement. Nature **446**(7137), 774–777 (2007)
9. A. Acín, E. Bagan, M. Baig, L. Masanes, R. Muñoz Tapia, Multiple-copy two-state discrimination with individual measurements. Phys. Rev. A, **71**, paper no. 032338 (2005)
10. A. Assalini, N. Dolla Pozza, G. Pierobon, Revisiting the Dolinar receiver through multiple-copy state discrimination theory. Phys. Rev. A **84**, paper no. 022342 (2011)
11. J. Geremia, Distinguishing between optical coherent states with imperfect detection. Phys. Rev. A **70**, paper no. 062303 (2004)
12. E. Parzen, *Stochastic Processes* (Holden Day, San Francisco, 1962)
13. M. Sasaki, O. Hirota, Optimum decision scheme with a unitary control process for binary quantum-state signals. Phys. Rev. A **54**, 2728–2736 (1996)
14. K. Kato, M. Osaki, M. Sasaki, O. Hirota, Quantum detection and mutual information for QAM and PSK signals. IEEE Trans. Commun. **47**(2), 248–254 (1999)
15. S. Izumi, M. Takeoka, M. Fujiwara, N.D. Pozza, A. Assalini, K. Ema, M. Sasaki, Displacement receiver for phase-shift-keyed coherent states. Phys. Rev. A **86**, paper no. 042328 (2012)
16. S. Izumi, M. Takeoka, K. Ema, M. Sasaki, Quantum receivers with squeezing and photon-number-resolving detectors for M-ary coherent state discrimination. Phys. Rev. A **87**, paper no. 042328 (2013)
17. G. Cariolaro, G. Pierobon, Theory of quantum pulse position modulation and related numerical problems. IEEE Trans. Commun. **58**(4), 1213–1222 (2010)
18. S.J. Dolinar, A near-optimum receiver structure for the detection of M-ary optical PPM signals. NASA, Technical Report 42–72, 1982
19. S.J. Dolinar, A class of optical receivers using optical feedback. Ph.D. dissertation, Department of Electrical Engineering and Computer Science, MIT, Cambridge (MA), 1976
20. S. Guha, J.L. Habif, M. Takeoka, Approaching Helstrom limits to optical pulse-position demodulation using single photon detection and optical feedback. J. Mod. Opt. **58**(3–4), 257–265 (2011)
21. J. Chen, J.L. Habif, Z. Dutton, R. Lazarus, S. Guha, Optical codeword demodulation with error rates below the standard quantum limit using a conditional nulling receiver. Nat. Photon. **6**(6), 374–379 (2012)
22. N. Dalla Pozza, N. Laurenti, Adaptive discrimination scheme for quantum pulse-position-modulation signals. Phys. Rev. A **89**, paper no. 012339 (2014)